Hindawi Publishing Corporation
Mathematical Problems in Engineering
Volume 2012, Article ID 351759, 22 pages
doi:10.1155/2012/351759

Research Article

Application of Periapse Maps for the Design of Trajectories Near the Smaller Primary in Multi-Body Regimes

Kathleen C. Howell, Diane C. Davis, and Amanda F. Haapala

School of Aeronautics and Astronautics, Purdue University, Armstrong Hall, West Lafayette, IN 47907, USA

Correspondence should be addressed to Kathleen C. Howell, howell@purdue.edu

Received 15 July 2011; Accepted 4 September 2011

Academic Editor: Antonio F. Bertachini A. Prado

The success of the Genesis spacecraft, as well as the current Artemis mission, continue to generate interest in expanding the trajectory options for future science and exploration goals throughout the solar system. Incorporating multi-body dynamics into the preliminary design can potentially offer flexibility and influence the maneuver costs to achieve certain objectives. In the current analysis, attention is focused on the development and application of design tools to facilitate preliminary trajectory design in a multi-body environment. Within the context of the circular restricted three-body problem, the evolution of a trajectory in the vicinity of the smaller primary is investigated. Introduced previously, periapse Poincaré maps have emerged as a valuable resource to predict both short- and long-term trajectory behaviors. By characterizing the trajectories in terms of radius and periapse orientation relative to the P_1-P_2 line, useful trajectories with a particular set of desired characteristics can be identified and computed.

1. Introduction

Spacecraft exploration activities increasingly involve trajectories that reach the vicinity of the libration points in various types of three-body systems. Libration point trajectories and low-energy transfers, in particular, have garnered much recent attention because of their potential to incorporate the natural dynamics, to generate new types of design options and, for some spacecraft applications, reduce propellant. A number of successful missions within the last decade have successfully exploited the natural dynamics of multiple gravity fields, for example, NASA's Genesis mission, launched in 2001 with a return to Earth in 2004 [1, 2]. In a Sun-Earth rotating view in Figure 1, the trajectory for the Genesis spacecraft leveraged the gravity of the Earth, Sun, and the Moon to supply a gravitational balance and

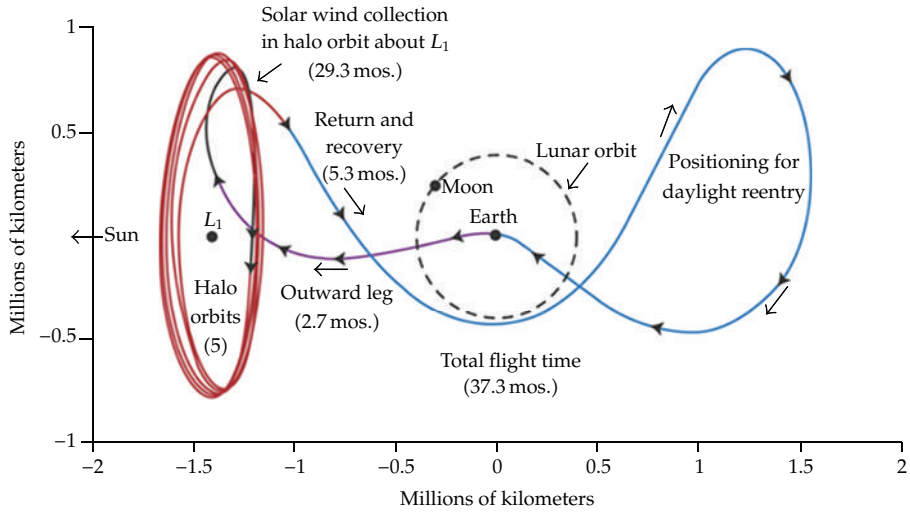

Figure 1: Genesis trajectory as viewed in the Sun-Earth rotating frame. Samples of solar material were collected on the spacecraft over two years in an L_1 libration point orbit and returned to Earth. During the return, the lunar gravity was also leveraged as the spacecraft shifted to the L_2 region prior to Earth reentry. CoutesyNASA/JPL-Caltech, http://genesismission.jpl.nasa.gov/gm2/mission/halo.htm.

deliver a trajectory that met the goals and satisfied the constraints with a path that does not emerge within the context of a two-body problem. In another example from an ongoing mission, Artemis involves two identical spacecraft identified as P1 and P2, originally two of the five Themis spacecraft [3–5]. Employing the Sun-Earth-Moon multi-body dynamical environment, these two vehicles were directed from the outermost of five elliptical Earth orbits to eventually arrive in Earth-Moon libration point orbits on August 25, 2010, and October 10, 2010. The transfer phase appears in Figure 2(a) as viewed in the Sun-Earth rotating fame; both spacecraft are to be inserted into elliptical lunar orbits (see Figure 2(b)) on June 27 and July 17, 2011, respectively.

Although much has been learned about the design space for such missions in the last few decades, as is evident from Genesis and Artemis as well as a number of other libration point missions, trajectory design in this type of regime remains a nontrivial problem. Typical challenges in the use of non-Keplerian orbits in a multi-body environment include (i) complexity: there are many destinations and competing goals; (ii) the search for solutions in new dynamical environments with frequent attempts to blend arcs from various models with different levels of fidelity; (iii) new types of scenarios that are explored to offer options for extended missions and contingencies. To exploit the gravity of multiple bodies requires a capability to deliver the trajectory characteristics that meet the requirements for a particular mission. Without analytical solutions, increasing insight into the dynamical structure in the three-body problem has been developed, beginning with Hénon and resulting in a wide variety of investigations, frequently with a focus toward applications [6–27]. In many of these analyses, the invariant manifolds associated with the L_1 and L_2 Lyapunov orbits have been increasingly used to predict the behavior of trajectories that originate near the smaller primary in the circular restricted three-body problem. In addition, the use of Poincaré maps to identify trajectories with various short- and long-term behaviors is effective. As noted in some of these recent publications, however, a major barrier to the development of a simple orbit

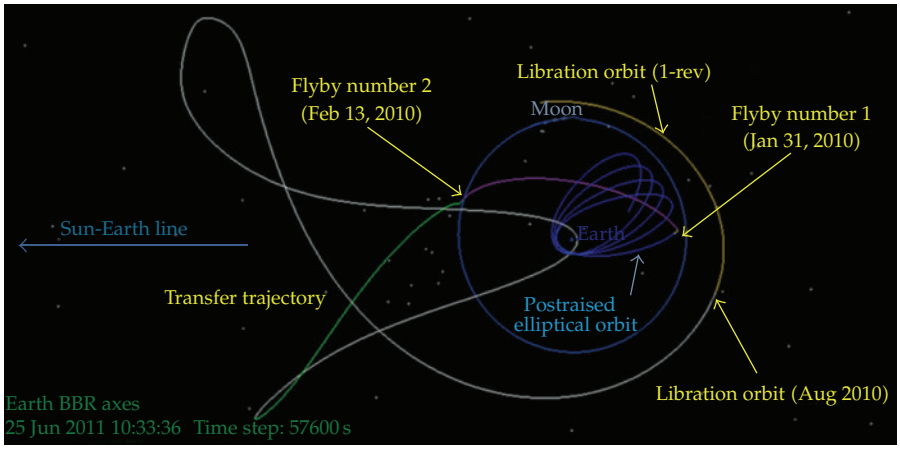

(a)

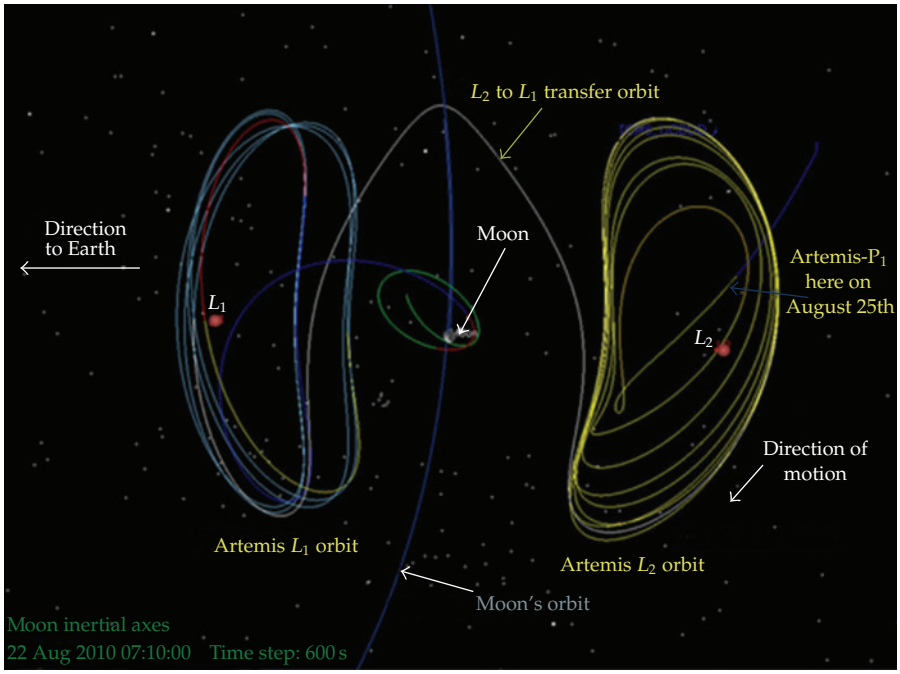

(b)

Figure 2: (a) Artemis trajectory for one spacecraft during transfer from Earth to lunar vicinity viewed in the Sun-Earth rating frame. The trajectory reaches the vicinity of the Sun-Earth L_1 libration point after two relatively high energy lunar flybys (a trajectory "backflip") to eventually reach a low-energy trajectory in the vicinity of the Moon. http://www.nasa.gov/mission_pages/artemis/news/lunar-orbit.html. (b) Artemis trajectory at arrival in lunar vicinity viewed in Earth-Moon rotating frame. Both spacecraft employ Earth-Moon L_1 and L_2 libration point orbits to modify the path and eventually insert into lunar orbit later this year. http://www.nasa.gov/mission_pages/artemis/news/lunar-orbit.html.

design process is the overwhelming nature of the design space. The trajectory design process remains challenging due to the varied, and sometimes chaotic, nature of trajectories that are simultaneously influenced by two gravitational bodies. To effectively select a trajectory to satisfy a given requirement, it is necessary to simplify and organize the design space as much as possible. The invariant manifold structure associated with the collinear libration points, in particular, has offered a geometrical framework for this dynamical environment. Yet, harnessing this information to supply relatively quick and efficient options for trajectory designers is a formidable challenge. Thus, the design difficulties remain significant, but a wider range of tools is emerging.

The motivation for this investigation originated from a general need to repeatedly develop design concepts for potential applications. A major challenge involved in orbit design within the context of the circular restricted three-body problem (CR3BP) is the organization of the vast set of options that is available within the design space; it is difficult to locate the specific initial conditions that lead to a trajectory with a particular set of characteristics. The invariant manifolds and the corresponding phase space yield a rich dynamical structure, and one method for visualizing the space involves the use of Poincaré maps, which reduce the dimensionality of the problem. Such maps are successfully employed in a number of analyses including Koon et al. [11, 12], Gómez et al. [13, 17], Howell et al. [14], Topputo et al. [18], and Anderson and Lo [27]. However, an alternative representation is sought to capture this knowledge and further facilitate trajectory design. A different parameterization of a Poincaré map involves the surface of section at the plane corresponding to periapsis. Its advantage is based on the fact that the map is viewed within position space. This type of map is denoted by a periapse Poincaré map and was first defined and introduced by Villac and Scheeres [28] to relate a trajectory escaping the vicinity of P_2 back to its previous periapsis in the planar Hill problem. Paskowitz and Scheeres [29, 30] extend this analysis, using periapse Poincaré maps to define lobes corresponding to the first four periapse passages after capture into an orbit about P_2. For application to the Europa orbiter problem, the authors define "safe zones" where a spacecraft is predicted to neither escape nor impact the surface of the satellite for a specified period of time. Davis and Howell [31, 32] build on the analysis for short- and long-term trajectories to illustrate some of the structures associated with manifold tubes corresponding to the L_1 and L_2 Lyapunov orbits as viewed in terms of periapse maps. Long-term periapsis Poincaré maps aid in organizing large numbers of trajectories and can deliver initial conditions that yield trajectories with specific characteristics. Davis and Howell [32] as well as Haapala and Howell [33] employ such maps to compute specific types of trajectories in the region near P_2. For trajectory design in this regime, good initial guesses are critical and a technique that supplies geometrical insight concerning the structure and delivers good approximate solutions is a practical alternative to construct trajectory options. Poincaré maps generally do require large amounts of computation, but such capabilities are expanding very quickly. In addition, as more design is accomplished within an interactive visual environment, techniques that are easily adaptable to visual interfaces are appealing and likely to be incorporated into the next generation of design tools. Ultimately, any of the design approaches that successfully leverage computational speed and visual interfaces possess advantages.

This analysis is focused on exploring periapse maps to construct trajectory options in multi-body regimes. The CR3BP frequently serves as a basis for the preliminary analysis in such problems, and, thus, for this investigation, the primary focus is the region near the smaller primary, P_2. The goal is a strategy that facilitates preliminary trajectory design in the CR3BP but still embraces the invariant manifold framework. Periapse Poincaré maps are

defined and the structure that is apparent in such types of maps is summarized. The map appears in position space, and different parameters at periapsis are represented depending on the application. Examples serve to demonstrate how the maps can be exploited to deliver different types of solutions. Periapse maps can also be used in conjunction with other types of analysis tools. Such an approach has proved useful to isolate specific arcs and, in some cases, blend them with other arcs for design.

2. Background

2.1. Dynamical Model

The dynamical model that is assumed for this analysis is consistent with the formulation in the circular restricted three-body problem (CR3BP), where the motion of a particle of infinitesimal mass, P_3, is examined as it moves in the vicinity of two larger primary bodies, P_1 and P_2. A rotating frame, centered at the system barycenter, B, is defined such that the rotating $\hat{x}$-axis is directed from the larger primary (P_1) to the smaller (P_2), the $\hat{z}$-axis is parallel to the direction of the angular velocity of the primary system with respect to the inertial frame, and the $\hat{y}$-axis completes the dextral orthonormal triad. Let the nondimensional mass μ be the ratio of the small mass of P_2 to the total system mass. The system then admits five equilibrium solutions comprised of the three collinear points (L_1, L_2, and L_3) and two equilateral points (L_4 and L_5) as depicted in Figure 3(a). Note that the magnitude of the Hill radius [8] is

$$r_H = \left(\frac{\mu}{3}\right)^{1/3}, \tag{2.1}$$

and is nearly equal to the distance between P_2 and the Lagrange points L_1 and L_2. A single integral of motion exists in the CR3BP. Known as the Jacobi integral, it is evaluated as

$$C = x^2 + y^2 + \frac{2\mu}{r_{23}} + \frac{2(1-\mu)}{r_{13}} - v^2, \tag{2.2}$$

where v is the magnitude of the spacecraft velocity relative to the rotating frame. The scalar nondimensional distances r_{13} and r_{23} reflect the distance to P_3 from the primaries P_1 and P_2, respectively. Then, the Jacobi constant restricts the motion of the spacecraft to regions in space, where $v^2 \geq 0$; these regions are bounded by surfaces of zero velocity. In the planar problem, the surfaces reduce to the zero velocity curves (ZVCs). For values of the Jacobi integral higher than that associated with the L_1 libration point, the ZVCs form closed regions around the two primaries. As the energy of the spacecraft is increased, the Jacobi value decreases until, at the L_1 value of the Jacobi integral, that is, C_{L_1}, the ZVCs open at the L_1 libration point, exposing a gateway. The particle P_3 is now free to move between the two large primaries. Similarly, when the value of the Jacobi integral decreases to the value associated with L_2, C_{L_2}, the ZVCs open at L_2 and the particle, that is, spacecraft, may escape entirely from the vicinity of the primaries. For values of such that $C_{L_3} < C < C_{L_2}$, the ZVCs appear as in Figure 3(b); the gray area cannot be reached by P_3 at this Jacobi level and is thus "forbidden."

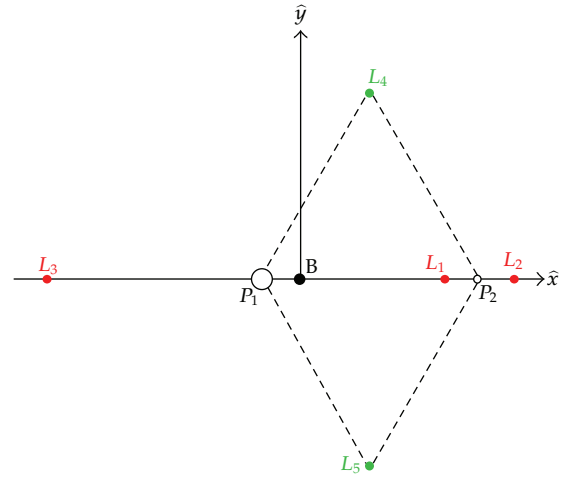

(a) Schematic of libration points

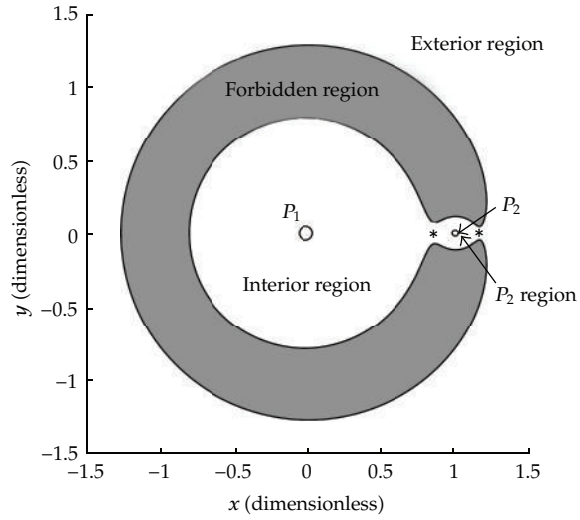

(b) Sample ZVC

Figure 3: Regions of position space delineated by the zero velocity curves.

The exterior and interior regions in the figure are denoted to be consistent with Koon et al. [11].

2.2. *Invariant Manifolds*

For unstable periodic orbits in the CR3BP, in particular the periodic Lyapunov orbits in the planar problem, higher-dimensional manifold structures exist and supply a framework for this region via the stable and unstable manifolds. For L_1 and L_2 Lyapunov orbits to exist at a given level of Jacobi constant, both the L_1 and L_2 gateways are open. Let t_o be the initial time and the symbol T identify the time for one period. Assume that $\lambda_s < 1$ and $\lambda_u = 1/\lambda_2$ are the stable and unstable eigenvalues from the monodromy matrix, $\Phi(t_o + T, t_o)$, as determined for

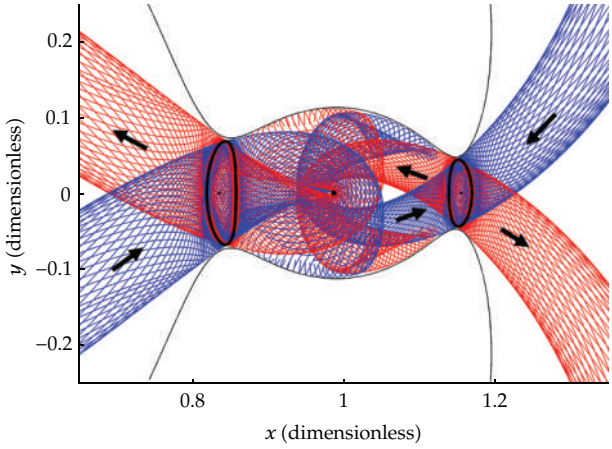

Figure 4: Stable (blue) and unstable (red) manifolds associated with periodic L_1 and L_2 Lyapunov orbits for $C = 3.1672$ in the Earth-Moon three-body problem.

a given Lyapunov orbit. Let $\overline{w}_s$ and $\overline{w}_u$ be the associated eigenvectors, computed by solving the equation $\Phi(t_o + T, t_o)\,\overline{w}_s = \lambda_s \overline{w}_s$, $\Phi(t_o + T, t_o)\,\overline{w}_u = \lambda_u \overline{w}_u$. Define $\overline{w}^+$, $\overline{w}^-$ as the two directions associated with an eigenvector. The local half-manifolds, W^{U-}_{loc} and W^{S-}_{loc}, are approximated by introducing a perturbation relative to a fixed point, $\overline{x}^*$, along the periodic orbit in the direction $\overline{w}^-_u$ and $\overline{w}^-_s$, respectively. Likewise, a perturbation relative to $\overline{x}^*$ in the direction $\overline{w}^+_u$ and $\overline{w}^+_s$, respectively, produces the local half-manifolds W^{U+}_{loc} and W^{S+}_{loc}. The step along the direction of the eigenvector is denoted d and the initial states along the local stable and unstable manifolds are evaluated as $\overline{x}^{\pm}_s = \overline{x}^* \pm d \cdot \overline{w}^{\pm}_s$. The local stable manifolds are globalized by propagating the states $\overline{x}^+_s$ and $\overline{x}^-_s$ in reverse time in the nonlinear model. This process yields the numerical approximation for the global manifolds $W^{S+}_{\overline{x}^*}$ and $W^{S-}_{\overline{x}^*}$, respectively. Propagating the state $\overline{x}^{\pm}_u = \overline{x}^* \pm d \cdot \overline{w}^{\pm}_u$ in forward-time yields the unstable global manifolds $W^{U+}_{\overline{x}^*}$ and $W^{U-}_{\overline{x}^*}$. The collection of the stable and unstable manifolds corresponding to each fixed point along sample L_1 and L_2 Lyapunov orbits in the Earth-Moon system appear in Figure 4 in configuration space.

3. Periapse Poincaré Maps

3.1. Creation of Periapse Maps

Connecting arcs in the CR3BP by exploiting the invariant manifold structures and the use of Poincaré maps has been successfully demonstrated by Koon et al., Gómez et al., and others [11–14, 16, 17]. A Poincaré map is commonly used to interpret the behavior of groups of trajectories, relating the states at one point in time to a future state forward along the path. By fixing the value of the Jacobi integral and selecting a surface of section, the dimensionality of the problem is reduced by two; the four-dimensional planar problem is thus reduced to two dimensions. Poincaré maps, with various parameterizations, have proven to be a useful tool for trajectory analysis and design. An alternative parameterization that facilitates exploration of the design space and selection of certain types of characteristics is the periapse Poincaré map, first defined and applied by Villac and Scheeres [28]. In this type of map, the surface of section is the plane of periapse passage. Villac and Scheeres, [28] as well as Paskowitz and

Scheeres, [29] employ periapse Poincaré maps to explore the short-term behavior of escaping trajectories as well as captured trajectories within the context of the Hill three-body problem with applications to the Jupiter-Europa system. Building on these results, the short- and long-term behavior of trajectories in the CR3BP as viewed in terms of periapse maps is explored by Davis and Howell [31, 32] as well as Haapala and Howell [33]. Periapsis and apoapsis relative to P_2 are defined such that the radial velocity, $\dot{r}$, of P_3 relative to P_2 is zero and are distinguishable by the direction of radial acceleration, $\ddot{r} \geq 0$ at periapsis and $\ddot{r} \leq 0$ at apoapsis [34].

The periapse maps are relatively simple to create. Each point within the periapse region corresponds to an initial condition that is associated with a specific trajectory about P_2 at a specified level of Jacobi constant. The initial condition always reflects a periapsis. Given an initial position, velocity can be selected to produce a prograde or retrograde path; all initial velocities are assumed prograde in this analysis. The initial state corresponding to each trajectory is then propagated forward in time for a specified number of revolutions to generate a series of subsequent periapse points. After the first revolution, the state is evaluated against four possible outcomes: the particle impacts P_2, the particle escapes out the L_1 gateway; the particle escapes through the L_2 gateway, or the particle remains captured near P_2, that is, it continues to evolve within the ZVCs. Impact trajectories are defined as those possessing a position vector, at any time, that passes on or within the radius of the body P_2. Escape trajectories are identified by an x-coordinate lying more than 0.01 nondimensional units beyond either L_1 or L_2. Finally, the initial periapse position is colored consistent with the outcome. Any states that continue to evolve are evaluated after the return to the next periapse condition and the process continues until a predetermined time or number of revolutions. Thus, maps are created to isolate certain types of behavior. Maps are produced in the Sun-Saturn system for both short- and long-term propagations in Davis and Howell [32] and Haapala and Howell [33]. Once a region is isolated, relationships between other periapsis parameters are also exploited [32, 33].

3.2. Defining Regions in the Maps

As an example, the periapse structures in the Sun-Saturn system, associated with the invariant manifolds corresponding to the planar Lyapunov orbits and a specified Jacobi constant value, appear in Figure 5. Note that the Sun and Saturn are simply a representative system. The manifolds in Figure 5(a) are propagated through their first periapses which are indicated as blue points along the manifold trajectories. Observe that the periapses along the manifold tubes define well-defined lobes that identify the escaping trajectories. These lobes are analogous to the lobes defined for the Hill restricted three-body problem in Villac and Scheeres [28] and Paskowitz and Scheeres [29]. Consistent with the nature of the stable/unstable manifolds that are associated with the Lyapunov orbits as separatrices for the flow, these lobes represent regions in which a periapsis occurs just prior to direct escape from the vicinity of Saturn; any trajectory with a periapsis within one of these lobes escapes prior to reaching its next periapsis. Conversely, a trajectory with periapsis lying outside a lobe does not escape before its next periapse passage. These lobes can, therefore, be considered gateways to escape: all escaping trajectories pass through one of these regions at the final periapse passage prior to escape. (Note that, for some trajectories, the first periapsis actually occurs in the vicinity of the libration point orbit near L_1 or L_2, however, these periapses are neglected in this investigation.) The boundaries of the lobes, that is, the periapses along the manifolds, appear as contours in Figure 5(a). To isolate the structures in the figure, a naming

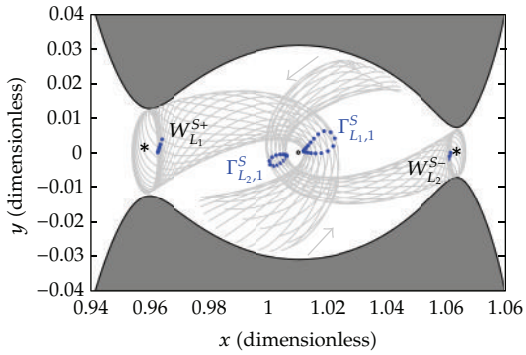

(a) Map of first periapses along WL1S+ and WL2S- for C=3.0173 (blue dots)

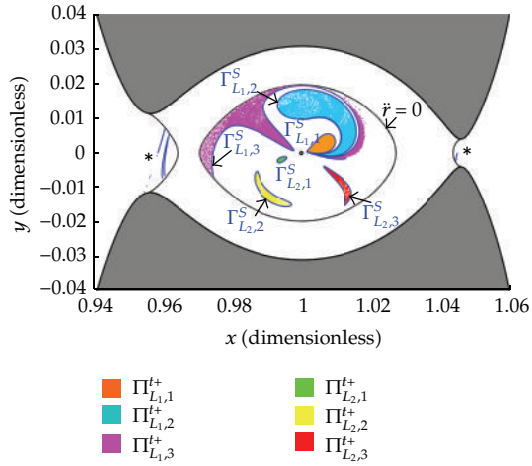

(b) First three periapses along $W^{S+}_{L_1}, W^{S-}_{L_2}$, and along L_1 forward-time escapes, and L_2 forward-time escapes for $C = 3.0174$

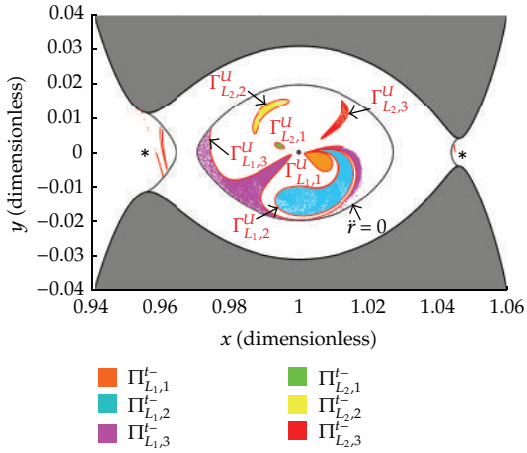

(c) First three periapses along $W^{U+}_{L_1}, W^{U-}_{L_2}$ and L_1 reverse-time escapes, and L_2 reverse-time escapes for $C = 3.0174$

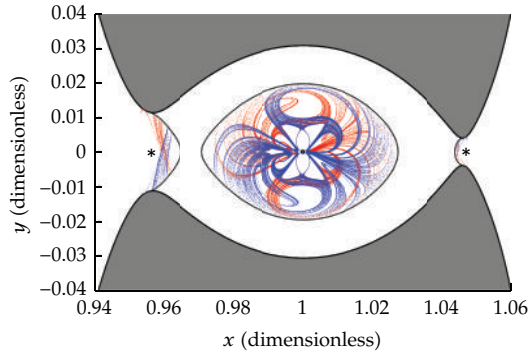

(d) Long-term periapse map associated with $W^{S+}_{L_1}$ (blue) and $W^{U-}_{L_2}$ (red) for $C = 3.0174$

Figure 5: Manifold and periapse structures in the Sun-Saturn system.

convention similar to one that appears in Koon et al. and Gómez et al. [11, 17] is employed. Let $\Gamma^S_{L_i,m}$ denote the periapse contour formed by the mth intersection of the stable manifold tube associated with the L_i Lyapunov orbit in the P_2 region, and $\Gamma^U_{L_j,n}$ denote the periapse contour formed by the nth intersection of the unstable manifold tube associated with the L_j Lyapunov orbit in the P_2 region. Then, to examine a periapse Poincaré map, consider the map in Figure 5(b). For the Lyapunov orbits at the given value of Jacobi constant, the first three periapses along each manifold $W^{S+}_{L_1}$ and $W^{S-}_{L_2}$ appear, as marked by blue dots in the figure, and distinct regions appear. Recall that the delineation between regions of allowed periapses and apoapses occur where $\ddot{r} = 0$, and this boundary is plotted as a dotted black line in the figures. Then, for a large number of arbitrary initial periapse locations, escaping trajectories are examined in both forward and reverse time. Those trajectories that cross

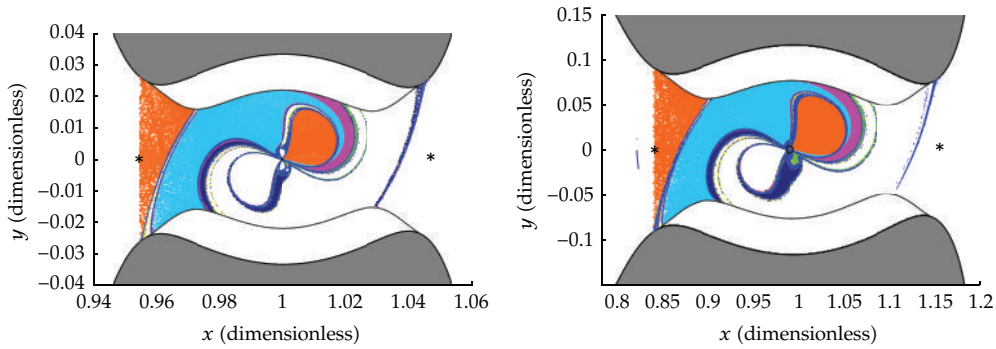

(a) Sun-Saturn system; $\mu = 2.858 \times 10^{-4}$, $C = 3.016$ (b) Earth-Moon system; $\mu = 1.215 \times 10^{-2}$, $C = 3.160$

Figure 6: Comparison of periapse regions in different systems.

the boundary $x = x_{L_1} - 0.01$ are defined as forward-time L_1 escape trajectories, while those that cross $x = x_{L_2} + 0.01$ are defined as forward-time L_2 escapes. Colors represent the fate of these initial periapse states. The colored areas in Figure 5(b) identify the locations of the first three periapses along these L_1 and L_2 forward-time escape trajectories and are denoted $\Pi^{t+}_{L_1,1\to3}$, and $\Pi^{t+}_{L_2,1\to3}$, respectively, where superscript $t+$ indicates a forward-time escape. The map associated with the first three periapses along the unstable manifolds ($W^{U+}_{L_1}$ and $W^{U-}_{L_2}$) is simply the reflection of the stable manifold contours from Figure 5(b) across the $\hat{x}$-axis, as demonstrated in Figure 5(c), and represent entry or capture into the specified region. The colored areas in Figure 5(c) represent locations of the first three periapses along the L_1 and L_2 reverse-time escape trajectories and are denoted $\Pi^{t-}_{L_1,1\to3}$ and $\Pi^{t-}_{L_2,1\to3}$, respectively, where superscript $t-$ indicates reverse-time escape. Propagating $W^{S+}_{L_1}$ and $W^{U-}_{L_2}$ for a longer interval and plotting all the manifold periapses together, the periapse structures appearing in Figure 5(d) emerge. The patterns apparent in the colored periapse regions are a function of the mass ratio as well as the value of the Jacobi integral. However, due entirely to the structure of the invariant manifolds associated with Lyapunov orbits, the patterns reappear in different systems as is apparent in Figure 6. The Sun-Saturn mass ratio is $\mu = 2.858 \times 10^{-5}$ as compared to the Earth-Moon system for which $\mu = 1.215 \times 10^{-2}$. The values of C differ, of course, but similar patterns are apparent in the two different systems as expected.

Ultimately, these maps represent pathways through the system. To highlight the paths that are available in this type of map, consider Figure 7, where both the Sun-Saturn and Earth-Moon systems are represented. In Figures 7(a) and 7(b), the regions corresponding to the first six periapses along L_1 forward-time escape trajectories are identified by color. Contours $\Gamma^{S}_{L_i,m}$ appear in blue for m within ~33 orbits of the primaries. The values of C in each system are selected for visual comparison and simply represent a similar opening of the gateway at L_2. Sample paths are over plotted on the maps and periapses are marked by dots in Figures 7(c) and 7(d). Assume that the initial periapsis occurs in the yellow region $\Pi^{t^+}_{L_1,6}$. The propagated path then moves to the next periapses in the green region ($\Pi^{t^+}_{L_1,5}$), and so on. The final periapsis occurs in the orange $\Pi^{t^+}_{L_1,1}$ region with a subsequent escape through L_1. In Figures 7(a) and 7(b), it is also apparent that some white regions exist. These are regions outside the lobes, that is, outside of the manifolds. Because the initial states in these white regions lie outside the manifolds, periapses in these regions can correspond to long-term behavior in the system. Not all white regions in Figure 7 correspond to long-term

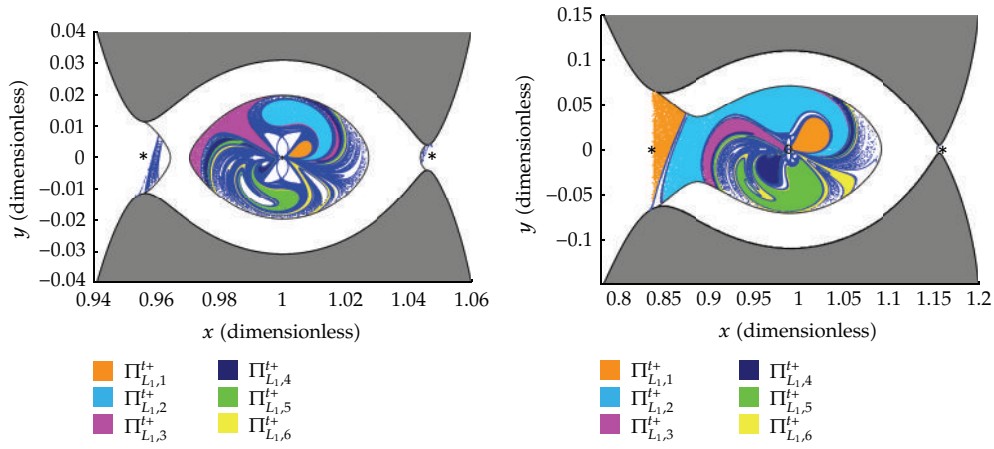

(a) Sun-Saturn escape map for six periapses at a value of Jacobi constant $C = 3.0174$

(b) Earth-Moon escape map for six periapses at a value of Jacobi constant $C = 3.17212$

(c) Sun-Saturn sequence originates with $\Pi^{t+}_{L_1,6}$ through $\Pi^{t+}_{L_1,1}$ to escape through the L_1 gateway

(d) Earth-Moon sequence originates with $\Pi^{t+}_{L_1,6}$ to escape through the L_1 gateway

Figure 7: Comparison of periapse maps for different Jacobi values and different systems.

capture in the vicinity of Saturn. At this value of Jacobi in the Sun-Saturn system, a relatively large white region appears near P_2 and a zoom of the same region near P_2 at $C = 3.0173$ appears in Figure 8. In Figure 8, the periapses along the manifold associated with the L_1 Lyapunov orbit appear in blue ($W^{S+}_{L_1}$) and those associated with the L_2 orbit appear in red ($W^{S-}_{L_2}$). The lobes reflecting escapes appear in white in Figure 8. The black dots correspond to periapses representing periodic orbits and other trajectories that evolve in this system for as long as 1000 years and it is apparent that there is significant structure in this long-term map. Numerous orbits and quasiperiodic trajectories that yield certain characteristics are selected directly from the map in Davis [35].

4. Applications of Periapse Maps

Exploiting Poincaré maps to construct trajectories has certainly been accomplished by others. Producing trajectories with certain characteristics can be facilitated with these types of periapse maps as well. Maps at different energy levels can also be employed together to blend

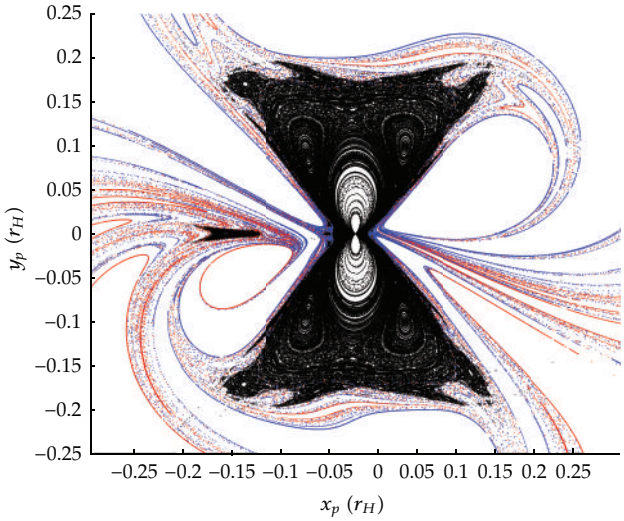

Figure 8: Long-term trajectories in a periapse Poincaré map; Sun-Saturn system; $C = 3.0173$.

arcs. Examples illustrating the process appear below. In some examples, known solutions emerge quickly.

4.1. Example: Transit through Both L_1 and L_2 Gateways

The unstable manifold tubes corresponding to the L_1 and L_2 Lyapunov orbits delineate regions in the periapse maps that correspond to trajectories that enter the vicinity of P_2 through the L_1 or L_2 gateways. As previously noted, the periapses of the unstable manifold trajectories are the mirror image (reflected across the $\hat{x}$-axis) of the stable manifold apses. A trajectory that lies both within a stable L_1 tube and an unstable L_2 tube can represent a "double transit" trajectory, that is, a trajectory that transits through both gateways. Such a trajectory enters the P_2 vicinity through L_2 and subsequently escapes, after an unspecified number of revolutions about P_2, through L_1 [11, 13, 17, 36]. For a particle to move from the exterior to the interior region requires such a path. Similarly, a transit trajectory may enter through the L_1 gateway and depart through L_2. A sample transit trajectory ($L_2 \rightarrow L_1$) appears in Figure 9 in the Sun-Saturn system. The first two lobes representing periapses within the L_2 unstable manifold appear in red; the first two lobes associated with the L_1 stable manifold appear in the figure in blue. A periapse state is selected that lies within both of the tubes; it appears as a black dot. Thus, the two lobes $\Pi^{t-}_{L_{2,2}}$ and $\Pi^{t+}_{L_{1,2}}$ overlap and the selected point appears in the intersection. The result is a transit trajectory that enters the vicinity of Saturn through L_2 and completes three periapse passages before escaping through the L_1 gateway, passing through three periapse lobes in sequence that highlight its passage. One advantage of the periapse Poincaré map for trajectory design applications is that the maps exist in configuration space, allowing the selection of initial conditions based on the physical location of periapsis. This type of application is explored in Davis and Haapala [35, 36].

Haapala and Howell [33] further explore the use of periapse Poincaré maps as a transit trajectory design tool. By selecting initial conditions that correspond to periapses within the region inside *both* contours $\Gamma^{S}_{L_i,m}$ and $\Gamma^{U}_{L_j,n}$, that is, within the intersections of regions $\Pi^{t+}_{L_i,m}$

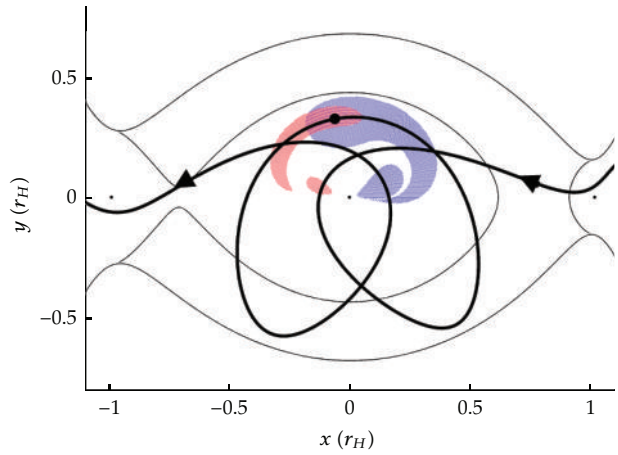

Figure 9: Transit from the exterior region to the interior region through gateways at both L_2 and L_1.

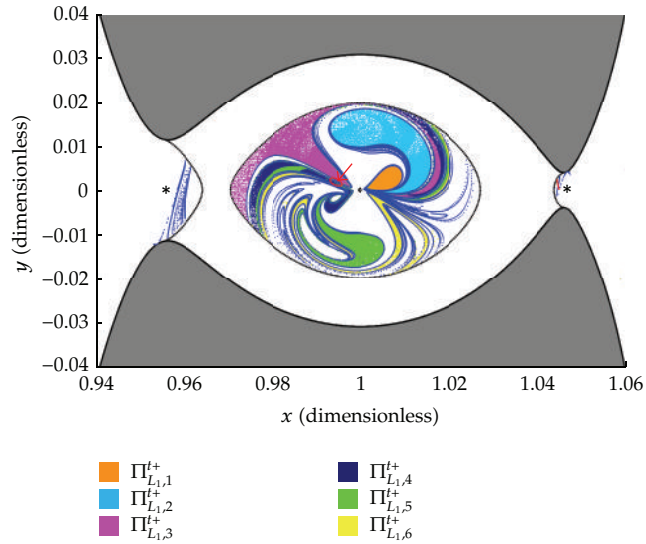

Figure 10: Arrival contour $\Gamma^{U}_{L_2,1}$ in red and contours $\Gamma^{S}_{L_1,1\to 10}$ in blue; $C = 3.0174$ (Saturn at 10x).

and $\Pi^{t-}_{L_j,n}$, and propagating in both forward- and reverse-time, a transit orbit passing through the L_i gateway in forward time, and the L_j gateway in reverse time is produced. Defining one revolution about P_2 as consisting of one periapsis and one apoapsis, the transit trajectory experiences a number of revolutions about P_2 equal to $p = m + n - 3/2$. Thus, to design transit trajectories with some desired behavior in the vicinity of P_2, the contours and/or intersections are selected such that $m + n = p + 3/2$, where for an Interior-to-Interior (I-to-I) transit $i = j = 1$, for an exterior-to-exterior (E-to-E) transit $i = j = 2$, for an Interior-to-Exterior (I-to-E) transit $i = 2$, $j = 1$, and lastly for an Exterior-to-Interior (E-to-I) transit $i = 1$, $j = 2$. Reconsider an E-to-I transfer using the map in Figure 10. After entering the L_2 gateway, all E-to-I transit trajectories reach their first periapses within the first contour $\Gamma^{U}_{L_2,1}$. Likewise, the last periapsis before exiting through the L_1 gateway occurs within the first

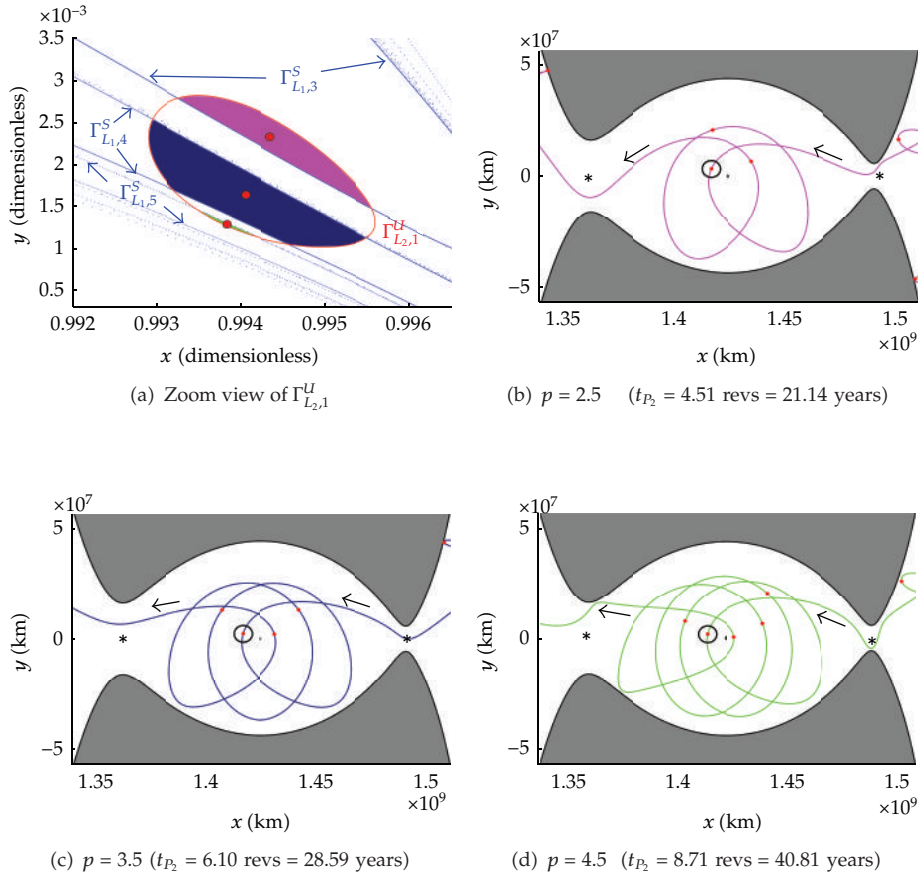

(a) Zoom view of $\Gamma^U_{L_2,1}$

(b) $p = 2.5$ ($t_{P_2} = 4.51$ revs = 21.14 years)

(c) $p = 3.5$ ($t_{P_2} = 6.10$ revs = 28.59 years)

(d) $p = 4.5$ ($t_{P_2} = 8.71$ revs = 40.81 years)

Figure 11: Transit trajectories of varying numbers of revolutions about Saturn appear with periapses marked in red.

contour $\Gamma^S_{L_1,1}$. Selecting $n = 1, m = 10$, it is possible to obtain trajectories with a maximum of $p = 9.5$ revolutions about P_2, although increasing n, m, or both could certainly render $p \geq 9.5$. The scenario from Figure 7(a) is repeated in Figure 10 but the manifold periapses are plotted for fewer crossings. The figure includes contours $\Gamma^S_{L_1,1\to 10}$ as blue dots, and $\Gamma^U_{L_2,1}$ as a contour in red (indicated by a red arrow). The six regions $\Pi^{t+}_{L_1,1\to 6}$ prior to escape out L_1 are colored appropriately. Within the red L_2 entry lobe, a certain structure is apparent when considering the intersections with the L_1 escaping contours as noted by Haapala and Howell [33] as well as Haapala [36]. Identifying the overlaps of the lobe regions yields transits that correspond to $p = 2.5,\ 3.5,\ 4.5$ and are colored in magenta, navy, and green in Figure 11(a). Note that the manifold contours at this particular value of Jacobi constant further split the arrival lobe into different subregions that reflect different types of E-to-I transit paths in terms of p, that is, the number of revolutions about P_2. Representative E-to-I transit trajectories are generated from the initial conditions marked as red points in Figure 11(a) and are plotted in Figures 11(b)–11(d). The time interval in the figures corresponds to the time required to pass from $x = x_{L_2}$ to $x = x_{L_1}$ and appears in the captions.

4.2. Example: Earth-Moon Transfers

Periapse Poincaré maps are also applied to the problem of designing a low-energy ballistic lunar transfer from low Earth orbit. Examined by various researchers [10, 12, 24, 37, 38], a ballistic lunar transfer utilizes the gravity of the Sun to naturally raise the periapsis of an Earth-centered trajectory, lowering the Δv required to reach the orbital radius of the Moon as compared to a Hohmann transfer. Initial condition or periapse maps simplify the problem of determining both the Δv and the orientation in the Sun-Earth frame that yield the appropriate periapse raise.

Consider a spacecraft in a 167 km circular parking orbit centered at Earth. At this energy level, the ZVCs are completely closed and the Sun has little effect on the orbit. A maneuver applied at an appropriate location in the parking orbit decreases Jacobi Constant and shifts the spacecraft to periapsis of a large Earth-centered orbit. This larger orbit is affected significantly by the Sun, and the subsequent periapsis is raised to the radius of the lunar orbit. If R_{E} is the radius of the Earth, to reach the Moon's orbital radius, the periapsis must be raised from R_{E} + 167 km to 384,400 km, corresponding to $\Delta r_p = 377,855\,\mathrm{km} = 0.2525\, r_H$, in terms of the Sun-Earth Hill radius. To determine the required Δv, periapse maps are created for a series of post-Δv Jacobi values. For each value of Δv, a Δr_p map is created. These maps allow a quick visualization of the orientation that produces the largest increase in periapse radius for each Δv. The ZVCs and the trajectories corresponding to approximately the largest periapse increase for a set of eight values of Δv appear in Figure 12(a). For $\Delta v < 3.199$ km/s, the ZVCs constrain the apoapsis to a radius too small to allow solar gravity to raise periapsis sufficiently. For $\Delta v \geq 3.2$ km/s, however, the ZVCs are sufficiently open (that is, the low value of Jacobi constant allows open gateways) to result in a periapse raise sufficiently large to reach the lunar orbit. This value agrees well with a theoretical minimum Δv determined by Sweetser [39] as 3.099 km/s for transfer from a 167-km parking orbit at Earth, as well as with optimized Earth-Moon transfer Δv values calculated by Parker and Born [38], who computes $\Delta v \approx 3.2$ km/s for a transfer from a 185 km parking orbit in a Sun-Earth-Moon gravity model.

A maneuver of 3.2 km/s shifts the value of Jacobi Constant from $C = 3.068621$, the value of C corresponding to the low-Earth orbit, to $C = 3.000785$ in the Sun-Earth system, the value of C associated with the transfer orbit. The postmaneuver initial condition map corresponding to $\Delta v = 3.2$ km/s, or $C = 3.000785$, appears in a full view in Figure 12(b) and a zoomed view in Figure 12(c); both are in the Sun-Earth rotating frame. The colors in Figures 12(b) and 12(c) simplify the options over the next revolution, that is, at this Jacobi constant, $C = 3.00078518$, depending on the location of the post-Δv periapsis along the parking orbit, the spacecraft can impact Earth (black) or escape the vicinity of the Earth entirely (red or blue). However, in this application, the focus is on the trajectories that remain in the vicinity of the Earth for at least one revolution, but with a significant rise in radius at the second periapsis. To locate the orientation for the appropriate periapse raise, a Δr_p map is produced. The map is recolored in Figure 12(d) to reflect the value of Δr_p over one revolution. Note that black indicates a decrease in Δr_p and blue $\rightarrow$ red indicates an increasing magnitude of Δr_p. The 167 km parking orbit is again marked in green on the map in Figure 12(d). Four bands of initial periapse angles exist that correspond to $\Delta r_p = 0.2525\, r_H$; these bands are marked by purple rays. By selecting an initial periapsis at the intersection of a purple ray with the green parking orbit, the orientation is determined that will result in the desired raise in periapsis. Four such trajectories appear in Figure 12(e) corresponding to the four initial conditions marked on the map in Figure 12(d). Clearly, each trajectory originates from

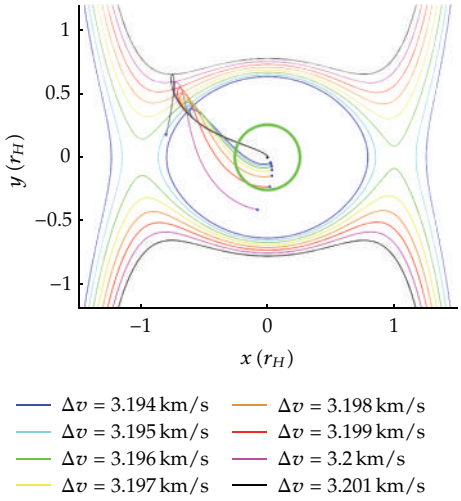

(a) Trajectories at a series of Δv values, each oriented for the largest periapse raise; lunar orbital radius marked in green

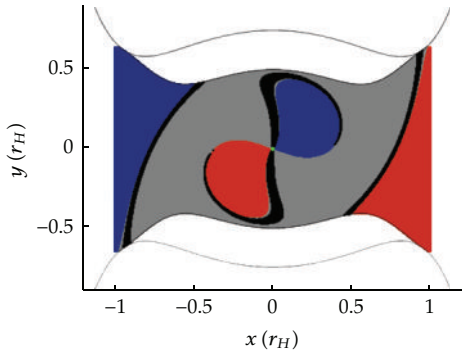

(b) Sun-Earth initial condition map corresponding to $C = 3.000785$

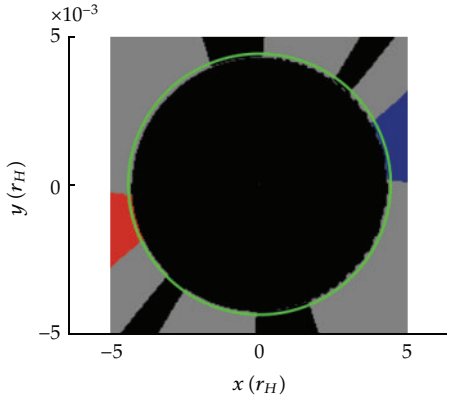

(c) Zoom near Earth; 167-km altitude; Earth orbit is green

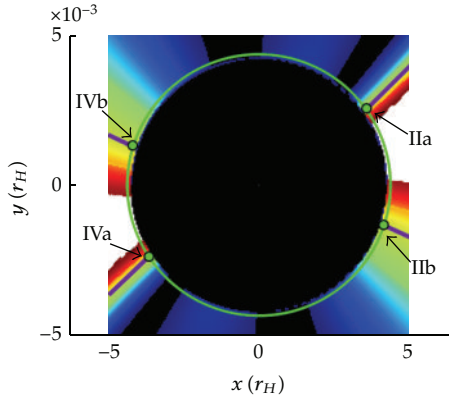

(d) Initial condition map colored in terms of Δr_p over one rev; desired Δr_p for Earth-Moon transfer denoted by purple rays; four selected ICs

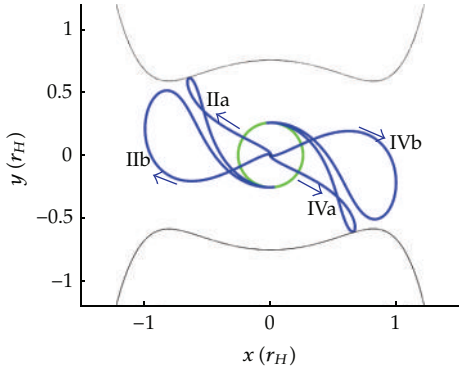

(e) Four Earth-Moon transfer trajectories correlated to selected points in map (d); Moon's orbit is green

Figure 12: Low-energy Earth-Moon transfer.

the 167-km parking orbit; after a $\Delta v = 3.2\,\mathrm{km/s}$, the trajectory reaches apoapsis well beyond the radius of the Moon's orbit. But the subsequent periapsis along each orbit is precisely at the radius of the Moon's orbit. Given that the data for the maps is available, computed ahead or in real time, the appropriate point is selected directly from the map; in a simple three-body model, the map is a fast easy method for preliminary design.

4.3. Example: Arrival through the L_1 Gateway

Sun-Saturn System

Consider arrivals in the vicinity of Saturn either by natural objects or spacecraft. The arrival lobe from either gateway can serve to deliver different types of arrival trajectories. Consider first an arrival through the L_1 gateway in the Sun-Saturn system as represented in Figure 13. The goal is an arrival periapsis that will produce a path that remains in the P_2 vicinity. In Figure 13(a), the arrival contour $\Gamma^{U}_{L_1,1}$ appears in red. Also plotted in the figure are the contours representing $\Gamma^{S}_{L_2,1\to n}$. In this example, the points within $\Pi^{t-}_{L_1,1}$ are colored based on time to escape from P_2 through either gateway, although not all trajectories escape within the time of propagation. Thus, periapses within the arrival region, $\Pi^{t-}_{L_1,1}$, are colored such that red $\to$ blue indicates increasing time to escape. Selection of a periapsis point that is in a region of the deepest blue color yields a trajectory that will remain in the P_2 vicinity for an extended time. Such a point is indicated in white with a white arrow in Figure 13(a). The corresponding path appears in Figure 13(b). Once propagated, it remains near Saturn for at least 1000 years. Arrival through L_2 could be accomplished with the same process.

Earth-Moon System

The same type of arrival lobe can yield a path for a different application in the Earth-Moon system in Figure 14. Many investigators have examined transfers from Earth to a periodic L_1 Lyapunov or halo orbit including Perozzi and Di Salvo [37] and Parker and Born [23]. The L_1 arrival contour for a given value of Jacobi Constant ($C = 3.17212$) appears in Figure 14(a). A periapsis is selected within this lobe (as indicated by the red dot and arrow) that also lies on a stable invariant manifold associated with the Lyapunov orbit. The selected lunar periapse point represents the gold trajectory arc in Figures 14(b) and 14(c). Earth departure occurs as a result of a maneuver, $\Delta v_1 = 3.105\,\mathrm{km/s}$, from a 200 km circular Earth parking orbit in black. The black arc then intersects the manifold (gold) corresponding to an L_1 Lyapunov orbit ($\Delta v_2 = 0.630\,\mathrm{km/s}$). After a close pass by the Moon at 100 km altitude, the path eventually asymptotically approaches the L_1 orbit as seen in Figures 14(b) and 14(c). The final result is a total $\Delta v = 3.735\,\mathrm{km/s}$ in the CR3BP. The periapsis is selected specifically to be along a manifold and is located on the blue contour $\Gamma^{S}_{L_1,1}$, however, this path could also produce a capture into a 100-km lunar orbit by including a 0.631 km/s maneuver at periapsis.

In Figure 15, the same objective is achieved with more excursions about the Moon prior to arrival in the L_1 orbit. Again, consider the arrival contour $\Gamma^{U}_{L_1,1}$ as plotted as the red lobe in Figure 14(a). Within this contour, select a periapsis from the green region, which represents the periapses corresponding to escaping trajectories from $\Pi^{t+}_{L_1,5}$. Propagating an initial condition from this region yields a path with four revolutions about the Moon prior to departure again through L_1. If the periapsis initial condition that is selected in the green region also lies on the contour $\Gamma^{S}_{L_1,5}$, as noted in the figure, the green trajectory arc in Figure 15

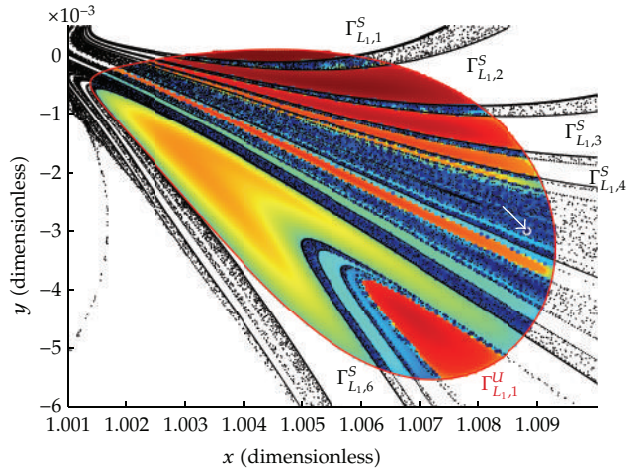

(a) Sun-Saturn system $C = 3.0174$; arrival contour $\Gamma^U_{L_1,1}$ overlaps with contours $\Gamma^S_{L_1,1\to m}$; escape periapses colored by time to escape

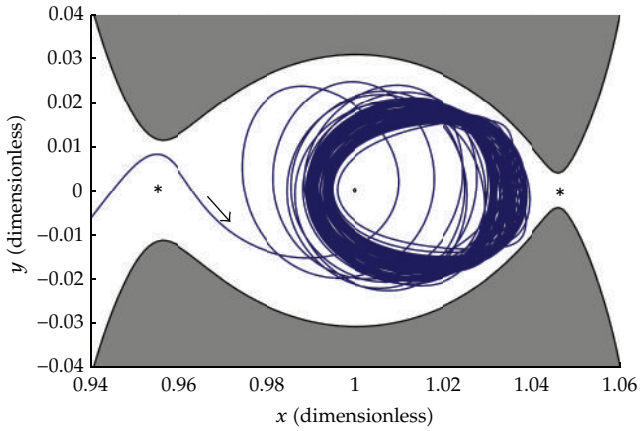

(b) Selection of arrival periapsis in deep blue region results in a path that remains in the vicinity of P_2 for over 1000 years

Figure 13: Arrival through the Sun-Saturn L_1 gateway; periapsis selected to yield a trajectory that remains in the P_2 vicinity for an extended time.

is generated. In comparison to the path in Figures 14(b) and 14(c), the green path in Figure 15 completes four revolutions about the Moon, passing the Moon at a higher altitude with a result that the total $\Delta v = 3.794\,\mathrm{km/s}$ with a corresponding increase in the time of flight. Other periapses yield opportunities to insert into alterative lunar trajectories as well.

5. Summary and Concluding Remarks

Trajectory design in the multi-body regime remains a nontrivial problem. The goal in any design process is to exploit the gravity of multiple bodies and deliver a trajectory with characteristics that meet the requirements for a particular mission. Without analytical solutions, increasing insight into the dynamical structure in the three-body problem

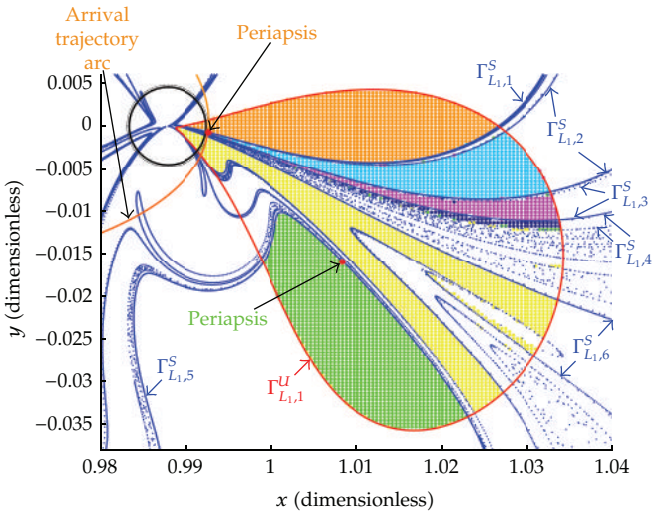

(a) Arrival contour $\Gamma^U_{L_1,1}$ and points within the lobe $\Pi^{t-}_{L_1,1}$ colored in terms of overlaps with regions $\Pi^{t+}_{L_1,1\to 6}$ as determined from contours $\Gamma^S_{L_1,1\to 6}$. A periapse point is selected (red dot) and the trajectory computed in forward and backward time from that periapsis (in gold)

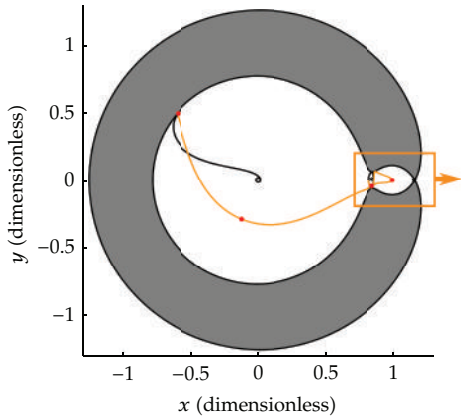

(b) Earth departure as a result of a maneuver from a 200-km circular parking orbit onto the black arc that intersects an L_1 Lyapunov orbit manifold

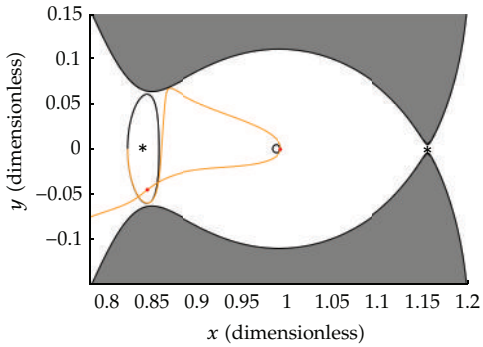

(c) Zoom: close pass by the Moon and approach to the Lyapunov orbit

Figure 14: Earth-Moon system $C = 3.17212$; manifold trajectory connects to the black arc that departs from 200-km altitude Earth orbit; lunar periapsis at 100-km altitude; asymptotic approach to L_1 Lyapunov orbit.

introduces more options for mission design as well as some new and exotic trajectories that may enable future opportunities. However, the design space is very large and the tradeoffs are not well defined. Many investigators are working to develop techniques to create viable solutions for applications. The invariant manifold structure associated with the collinear libration points, in particular, has supplied a geometrical framework and a number of approaches are now available to represent this information. This current analysis explores

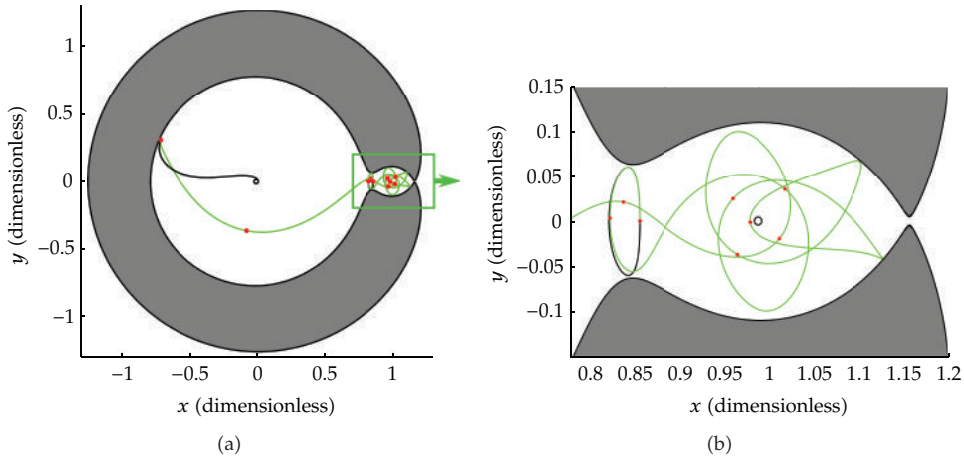

Figure 15: Earth-Moon system; $C = 3.17212$; manifold trajectory connects to the black arc that departs from 200-km altitude Earth orbit; asymptotic approach to L_1 Lyapunov orbit after four revolutions about the Moon.

an additional type of map to add another perspective for selecting arcs in support of the design process. Within the context of the CR3BP, the periapse maps are an efficient design tool. Using a combination of strategies to manage the information and deliver the results is almost always necessary, however, automating these techniques is a priority; a visual interface is a longer-term goal.

Acknowledgments

The authors wish to thank the Purdue University Graduate School, the College of Engineering, and the School of Aeronautics and Astronautics for support of this effort. Additional support is also appreciated through a GAANN Fellowship (Graduate Assistance in Areas of National Need), a Zonta International Amelia Earhart Fellowship, and a Purdue Forever Fellowship. Assistance for the computational facilities is provided through the Eliasen Visualization Laboratory. The paper has been presented at the 6th International Workshop and Advanced School "Spaceflight Dynamics and Control," Covilha, Portugal, March 28-30, 2011, http://www.aerospace.ubi.pt/workshop2011/.

References

[1] K. C. Howell, B. T. Barden, and M. W. Lo, "Application of dynamical systems theory to trajectory design for a libration point mission," *Journal of the Astronautical Sciences*, vol. 45, no. 2, pp. 161–178, 1997.

[2] M. W. Lo, B. G. Williams, W. E. Bollman et al., "Genesis mission design," *Journal of the Astronautical Sciences*, vol. 49, no. 1, pp. 169–184, 2001.

[3] V. Angelopoulos, "The THEMIS mission," *Space Science Reviews*, vol. 141, no. 1–4, pp. 5–34, 2008.

[4] V. Angelopoulos, "The ARTEMIS mission," *Space Science Reviews*. In press.

[5] M. Woodard, D. Folta, and D. Woodfork, "ARTEMIS: the first mission to the lunar libration points," in *Proceedings of the 21st International Symposium on Space Flight Dynamics*, Toulouse, France, September-October 2009.

[6] M. Hénon, "Exploration of the restricted problem. V. Hill's case: periodic orbits and their stability," *Astronomy and Astrophysics*, vol. 1, pp. 223–238, 1969.

[7] M. Hénon, "Exploration of the restricted problem. VI. Hill's case: non-periodic orbits," *Astronomy and Astrophysics*, vol. 9, pp. 24–36, 1970.

[8] D. P. Hamilton and J. A. Burns, "Orbital stability zones about asteroids," *Icarus*, vol. 92, no. 1, pp. 118–131, 1991.

[9] H. Yamakawa, J. Kawaguchi, N. Ishil, and H. Matsuo, "On earth-moon transfer trajectory with gravitational capture," in *Proceedings of the AAS/AIAA Astrodynamics Specialist Conference*, Victoria, Canada, August 1993, Paper No. AAS 93-633.

[10] E. A. Belbruno and J. K. Miller, "Sun-perturbed earth-to-moon transfers with ballistic capture," *Journal of Guidance, Control, and Dynamics*, vol. 16, no. 4, pp. 770–775, 1993.

[11] W. S. Koon, M. W. Lo, J. E. Marsden, and S. D. Ross, "Heteroclinic connections between periodic orbits and resonance transitions in celestial mechanics," *Chaos*, vol. 10, no. 2, pp. 427–469, 2000.

[12] W. S. Koon, M. W. Lo, J. E. Marsden, and S. D. Ross, "Low energy transfer to the moon," *Celestial Mechanics and Dynamical Astronomy*, vol. 81, no. 1-2, pp. 63–73, 2001.

[13] G. Gómez, W. S. Koon, M. W. Lo, J. E. Marsden, J. Masdemont, and S. D. Ross, "Invariant manifolds, the spatial three-body problem and space mission design," in *Proceedings of the AAS/AIAA Astrodynamics Specialist Conference*, Quebec, Canada, August 2001, Paper No. AAS 2001-301.

[14] K. C. Howell, B. G. Marchand, and M. W. Lo, "Temporary satellite capture of short-period Jupiter family comets from the perspective of dynamical systems," *American Astronautical Society. Journal of the Astronautical Sciences*, vol. 49, no. 4, pp. 539–557, 2001.

[15] A. F. Prado, "Third-body perturbation in orbits around natural satellites," *Journal of Guidance, Control, and Dynamics*, vol. 26, no. 1, pp. 33–40, 2003.

[16] F. Topputo, M. Vasile, and A. E. Finzi, "Combining two and three-body dynamics for low energy transfer trajectories of practical interest," in *Proceedings of the 55th International Astronautical Congress*, pp. 584–596, Vancouver, Canada, October 2004, IAC-04-A.7.02.

[17] G. Gómez, W. S. Koon, M. W. Lo, J. E. Marsden, J. Masdemont, and S. D. Ross, "Connecting orbits and invariant manifolds in the spatial restricted three-body problem," *Nonlinearity*, vol. 17, no. 5, pp. 1571–1606, 2004.

[18] F. Topputo, M. Vasile, and F. Bernelli-Zazzera, "Low energy interplanetary transfers exploiting invariant manifolds of the restricted three-body problem," *Journal of the Astronautical Sciences*, vol. 53, no. 4, pp. 353–372, 2005.

[19] R. L. Anderson and M. W. Lo, "Virtual exploration by computing global families of trajectories with supercomputers," in *Proceedings of the AAS/AIAA Spaceflight Mechanics Meeting*, Copper Mountain, Colo, USA, January 2005, Paper No. AAS 05-220.

[20] R. P. Russell, "Global search for planar and three-dimensional periodic orbits near Europa," *Journal of the Astronautical Sciences*, vol. 54, no. 2, pp. 199–226, 2006.

[21] C. F. de Melo and O. C. Winter, "Alternative paths to Earth-moon transfer," *Mathematical Problems in Engineering*, vol. 2006, Article ID 34317, 20 pages, 2006.

[22] F. García and G. Gómez, "A note on weak stability boundaries," *Celestial Mechanics and Dynamical Astronomy*, vol. 97, no. 2, pp. 87–100, 2007.

[23] J. S. Parker and G. H. Born, "Direct lunar halo orbit transfers," in *Proceedings of the 17th AAS/AIAA Space Flight Mechanics Conference*, Sedona, Ariz, USA, 2007, Paper AAS 07-229.

[24] J. S. Parker and G. H. Born, "Modeling a low-energy ballistic lunar transfer using dynamical systems theory," *Journal of Spacecraft and Rockets*, vol. 45, no. 6, pp. 1269–1281, 2008.

[25] G. A. Tsirogiannis, E. A. Perdios, and V. V. Markellos, "Improved grid search method: an efficient tool for global computation of periodic orbits," *Celestial Mechanics and Dynamical Astronomy*, vol. 103, no. 1, pp. 49–78, 2009.

[26] E. Belbruno, M. Gidea, and F. Topputo, "Weak stability boundary and invariant manifolds," *SIAM Journal on Applied Dynamical Systems*, vol. 9, no. 3, pp. 1061–1089, 2010.

[27] R. L. Anderson and M. W. Lo, "A dynamical systems analysis of resonant flybys: ballistic case," *The Journal of the Astronautical Sciences*, vol. 58, no. 2, 2011.

[28] B. F. Villac and D. J. Scheeres, "Escaping trajectories in the Hill three-body problem and applications," *Journal of Guidance, Control, and Dynamics*, vol. 26, no. 2, pp. 224–232, 2003.

[29] M. E. Paskowitz and D. J. Scheeres, "Robust capture and transfer trajectories for planetary satellite orbiters," *Journal of Guidance, Control, and Dynamics*, vol. 29, no. 2, pp. 342–353, 2006.

[30] M. E. Paskowitz and D. J. Scheeres, "Design of science orbits about planetary satellites: Application to Europa," *Journal of Guidance, Control, and Dynamics*, vol. 29, no. 5, pp. 1147–1158, 2006.

[31] D. C. Davis and K. Howell, "Long term evolution of trajectories near the smaller primary in the restricted problem," in *Proceedings of the 20th AAS/AIAA Space Flight Mechanics Meeting*, San Diego, Calif, USA, February 2010.

[32] D. C. Davis and K. Howell, "Trajectory evolution in the multi-body problem with applications in the saturnian system," in *Proceedings of the 61st International Astronautical Congress*, Prague, Czech Republic, September 2010.

[33] A. F. Haapala and K. C. Howell, "Trajectory design using Poincaré maps and invariant manifolds," in *Proceedings of the 21st AAS/AIAA Space Flight Mechanics Meeting*, New Orleans, La, USA, February 2011.

[34] B. F. Villac and D. J. Scheeres, "On the concept of periapsis in Hill's problem," *Celestial Mechanics and Dynamical Astronomy*, vol. 90, no. 1-2, pp. 165–178, 2004.

[35] D. C. Davis, *Multi-body trajectory design strategies based on periapsis Poincaré maps*, Ph.D. dissertation, School of Aeronautics and Astronautics, Purdue University, West Lafayette, Ind, USA, 2011.

[36] A. F. Haapala, *Trajectory design using periapsis Poincaré maps and invariant manifolds*, M.S. thesis, School of Aeronautics and Astronautics, Purdue University, West Lafayette, Ind, USA, 2011.

[37] E. Perozzi and A. Di Salvo, "Novel spaceways for reaching the Moon: an assessment for exploration," *Celestial Mechanics and Dynamical Astronomy*, vol. 102, no. 1–3, pp. 207–218, 2008.

[38] J. Parker and G. Born, "Targeting low-energy ballistic lunar transfers," in *Proceedings of the AAS George H. Born Symposium*, Boulder, Colo, USA, May 2010, Paper No. AAS 10-1859.

[39] T. H. Sweetser, "An estimate of the global minimum ΔV needed for earth-moon transfer," in *Proceedings of the AAS/AIAA Spaceflight Mechanics Meeting*, Houston, Tex, USA, February 1991, Paper No. AAS 91-101.